EMITOR: Jurnal Teknik Elektro

Simulation and Modeling CUK H-Bridge Current-Controlled Inverter Using a Proportional-Integral Algorithm

Fahrul Indra Setiyawan*, Eka Nuryanto Budisusila
Master of Electrical Engineering Industry – Universitas Islam Sultan Agung
Semarang, Indonesia
*fahrulindra56@gmail.com

Abstract – *The growing demand for renewable energy has increased the need for efficient and reliable power conversion systems, particularly for applications that require stable current control and good power quality. This paper presents the simulation and modeling of a CUK H-Bridge inverter with current control using a Proportional-Integral (PI) algorithm implemented in Power Simulator (PSIM) software. The proposed topology combines an H-Bridge inverter and a CUK AC–AC converter to enable bidirectional power flow, buck–boost voltage operation, and low Total Harmonic Distortion (THD) in the output current. The PI controller parameters are determined using the empirical Ziegler–Nichols (Z–N) method and further refined through fine-tuning to obtain optimal values of $K_p = 0.6$, $T_i = 0.0167$, and $K_i = 35$. Simulation results show that the actual output current (I_{act}) can accurately track the reference current (I_{ref}) with minimal steady-state error. The proposed inverter operates in buck mode ($V_o < V_{\text{in}}$), steady-state mode ($V_o \approx V_{\text{in}}$), and boost mode ($V_o > V_{\text{in}}$) according to the reference current value. A maximum output power of 2.25 kW is achieved at a reference current of 15 A with an output voltage of 150 V. The output current THD is 3.6%, which satisfies the IEEE 519 standard. These results indicate that the PI-controlled CUK H-Bridge inverter provides stable current tracking, flexible voltage regulation, and acceptable power quality for renewable energy applications.*

Keywords – *CUK Converter; H-Bridge Inverter; PI Controller; THD; PSIM.*

I. Introduction

RENEWABLE energy use is currently growing rapidly as the global energy sector moves toward cleaner, more sustainable, and environmentally friendly power generation systems. Hydropower, solar power, and wind power are some of the renewable energy sectors that are being extensively developed [1]. This development is driven by the large potential of renewable energy resources, which can reduce dependence on fossil fuels [2]. In addition, fossil fuel reserves are gradually decreasing and their utilization has a negative impact on the environment, making the transition to renewable energy increasingly necessary [3]. Renewable energy is also considered a promising source of future energy because it produces low emissions and is available in abundant quantities [4].

The utilization of renewable energy requires a power conversion system capable of processing the generated electrical energy so that it can be used by consumers or integrated into the electrical grid [5]. In renewable energy systems, especially those based on photovoltaic or DC sources, an inverter plays an important role in converting DC voltage into AC voltage [6]. In addition to voltage conversion, the inverter must also be able to inject current into the grid with good quality and stable characteristics. Therefore, the generated current must have low distortion, stable amplitude, and proper synchronization with the output voltage [7].

However, conventional single-phase and three-phase inverters still have several limitations. These limitations include the inability to produce a fully sinusoidal output voltage, high common-mode voltage, and non-continuous input current [8]. These conditions can reduce power quality and affect the performance of the connected load or grid system. One of the most common problems in inverter-based systems is Total Harmonic Distortion (THD), which indicates the level of harmonic content in the output waveform [9]. A high THD value may cause additional losses, heating, and reduced system reliability.

The H-bridge is one of the most widely used inverter topologies because of its simple structure and

The manuscript was received on June 2, 2026, revised on June 7, 2026, and published online on July 31, 2026. Emitor is a Journal of Electrical Engineering at Universitas Muhammadiyah Surakarta with ISSN (Print) 1411 – 8890 and ISSN (Online) 2541 – 4518, holding Sinta 3 accreditation. It is accessible at https://journals2.ums.ac.id/index.php/emitor/index.

ability to generate AC output using four power switches controlled by SPWM signals [10, 11]. Its high modularity makes it superior to several other inverter topologies, including its ability to reduce voltage clamping on each switching device [12, 13]. Nevertheless, the H-bridge inverter still requires an additional conversion stage when voltage regulation in both step-up and step-down modes is needed. For this reason, the integration of an H-bridge inverter with a buck-boost converter topology becomes an attractive solution for renewable energy applications.

The CUK converter is a variation of the buck-boost converter that can step up or step down the output voltage with good efficiency [14]. This converter also has the advantage of more continuous input and output currents due to the use of inductors and capacitors as energy storage elements. In addition, the CUK converter can be equipped with an LC filter to reduce THD in the output current [15]. These characteristics make the CUK converter suitable for applications that require stable voltage regulation and improved current quality.

Combining a CUK converter with an H-bridge inverter, known as a CUK H-bridge inverter, enables bidirectional power flow and can be applied to renewable energy systems [16]. This topology has the potential to provide flexible buck-boost voltage operation while maintaining better current quality. However, the performance of this topology strongly depends on the control strategy used to regulate the output current. A Proportional-Integral (PI) control algorithm is commonly used because it has a simple structure, fast response, and good accuracy in reducing steady-state error [17]. Therefore, PI-based current control becomes a relevant approach for improving the performance of the CUK H-Bridge inverter.

This study presents the simulation and modeling of a CUK H-Bridge Inverter with PI algorithm-based current control using Power Simulator (PSIM) software. Although several studies have discussed buck-boost inverter topologies, current control in the CUK H-Bridge Inverter topology has received limited attention in the existing literature [18]. Most previous studies have focused on voltage control or topology development, while the output current tracking performance and harmonic quality of the CUK H-Bridge inverter still require further investigation.

Based on the literature review, various buck-boost inverter topologies have been developed, ranging from the Switched-Coupled-Inductor Inverter and the One-Leg H-Bridge Inverter to the integration of the H-Bridge with SEPIC and Zeta converters. These developments have successfully improved step-up and step-down capabilities as well as output power quality. The comparative data of several H-bridge inverter developments are presented in Table 1.

Table 1: H-bridge inverter development

Topology	Control Method	Switches	THD
Switched-Coupled-Inductor DC-AC Inverter	Duty Cycle SPWM	3	–
One-Leg H-Bridge Inverter	PI + SPWM	4	3.65%
SEPIC H-Bridge Inverter	SPWM	8	4.50%
Zeta H-Bridge Inverter	PI + SPWM	6	1.10%
CUK H-Bridge Inverter	PI + Ziegler–Nichols + SPWM	8	3.60%

However, research on current control in the CUK H-Bridge Inverter topology remains limited. In fact, the CUK converter offers several advantages, such as buck-boost capability, more continuous input and output currents, and the potential to produce better power quality. As shown in Table 1, the CUK H-Bridge Inverter achieves a THD value of 3.60%, indicating that this topology has the potential to meet power quality requirements.

Therefore, this study proposes the modeling and simulation of the CUK H-Bridge Inverter with current control using a Proportional-Integral (PI) controller tuned using the Ziegler–Nichols method. Unlike previous studies, which generally focused on voltage control, this study emphasizes output current control to achieve a fast and stable response that meets power quality standards with a THD of 3.60%. The main contribution of this study is the development of a PI-controlled CUK H-Bridge inverter model that can operate in buck, steady-state, and boost modes while maintaining low harmonic distortion in the output current.

Thus, this study is expected to provide an alternative buck-boost inverter topology with a simple control strategy, good power quality, and suitability for renewable energy applications.

II. Research Methods

This section describes the research methodology used to model, simulate, and evaluate the proposed CUK H-Bridge current-controlled inverter. The discussion includes the basic principle of the CUK converter, H-Bridge inverter operation, current control strategy, PI controller design, PSIM simulation environment, proposed topology, and testing procedures.

i. CUK Converter

A CUK converter is a type of DC–DC converter that can be used to step up or step down the output voltage, as shown in Figure 1. This topology uses two inductors to reduce current ripple on both the input and output sides, while also producing a continuous current. When the switch in the CUK converter is in the closed or ON state, the coupling capacitor acts as an energy transfer medium and simultaneously delivers energy to the output inductor L_2 and the load [19].

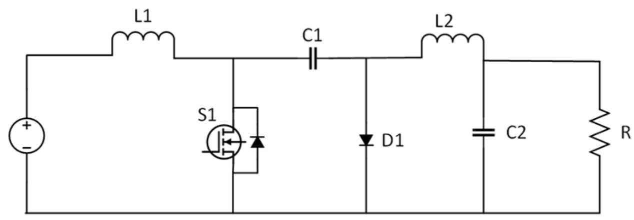

Figure 1: CUK converter.

Although the CUK converter offers several advantages, such as current stability and flexible voltage regulation, it requires a compensation circuit to maintain system stability [20]. The magnitude of the voltage ripple, denoted by ΔV, is proportional to the load current I and inversely proportional to the switching frequency f and capacitance C. The inductor L_1 on the input side acts as a DC voltage filter to reduce high harmonic components. Meanwhile, capacitor C_1 stores and transfers energy from the input side to the output side. When the MOSFET is in the OFF state, current flows through inductors i_{L1} and i_{L2} through the diodes [21].

After describing the CUK converter as the voltage regulation stage, the next subsection explains the H-Bridge inverter, which functions as the DC-to-AC conversion stage.

ii. H-Bridge Inverter

Figure 2 shows the H-Bridge inverter power circuit that uses four power switches. The input voltage V_{in} is supplied by a DC source, while the output voltage is connected to the CUK AC–AC converter circuit shown in Figure 4.

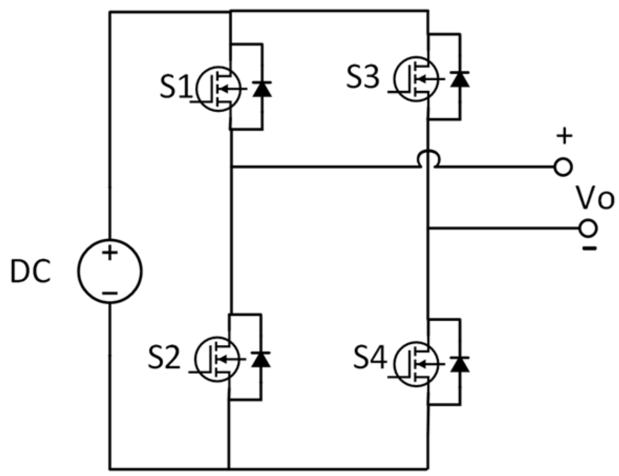

Figure 2: H-Bridge inverter.

The operating principle of the H-Bridge inverter can be analyzed based on its positive-cycle and negative-cycle switching modes. During the positive cycle, switches S_1 and S_3 are active. This condition allows current to flow from the V_{DC} source to L_1 and the load through S_3, resulting in a positive output voltage. The voltage relationship during this positive-cycle operation is expressed in Equation (1) [22, 23].

$$V_{\text{DC}} = V_L + V_{\text{out}} \tag{1}$$

By substituting the inductor voltage relationship into Equation (1), the positive-cycle voltage equation can be rewritten as shown in Equation (2).

$$V_{\text{DC}} = L\frac{di_L}{dt} + V_{\text{out}} \tag{2}$$

In the negative-cycle operation mode, switches S_2 and S_4 are active. In this condition, current from the V_{DC} source flows to the load through S_2 and returns through S_4 to the source. The voltage relationship during this negative-cycle operation is expressed in Equation (3) [22, 23].

$$-V_{\text{DC}} = V_L + V_{\text{out}} \tag{3}$$

By applying the same inductor voltage relationship, the negative-cycle voltage equation can be written as shown in Equation (4).

$$-V_{\text{DC}} = L\frac{di_L}{dt} + V_{\text{out}} \tag{4}$$

After the inverter operating principle has been described, the next subsection discusses the current control strategy required to regulate the output current of the proposed inverter system.

iii. Current Control in Inverter Systems

Current control is a critical aspect of modern inverter systems, particularly in applications requiring high stability and precision, such as electric motor drives, renewable energy systems, and DC-to-AC power conversion. Its main objective is to ensure that the inverter output current follows the reference signal quickly and accurately, while minimizing disturbances or ripple that may damage the load [24].

Current control techniques are divided into two main categories. The first category is linear current control, such as PI control, which operates based on the error between the reference current and the actual current. The second category is hysteresis control, which uses a switching method based on the upper and lower thresholds of the current signal. In inverter systems based on the CUK H-Bridge topology, current control becomes more precise due to the presence of energy storage elements such as inductors and capacitors [24].

After explaining the role of current control in inverter systems, the next subsection presents the PI algorithm used as the main control method in this study.

iv. PI Algorithm

A Proportional-Integral (PI) controller is a combination of proportional control and integral control, as shown in Figure 3. The proportional component K_p accelerates the system response but cannot eliminate steady-state error, whereas the integral component K_i eliminates steady-state error by integrating the error over time [25].

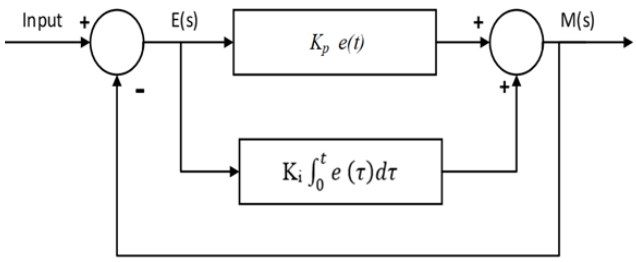

Figure 3: Proportional-Integral controller.

The control output of the PI controller in the time domain is determined by the proportional term and the integral term. The time-domain equation of the PI controller is expressed in Equation (5).

$$m(t) = K_p e(t) + K_i \int e(\tau)d\tau \tag{5}$$

To analyze the controller in the frequency domain, the PI controller can also be represented using the Laplace transform. The Laplace-domain transfer function of the PI controller is shown in Equation (6).

$$\frac{M(s)}{E(s)} = K_p\left(1+\frac{1}{T_i s}\right) \tag{6}$$

where K_p represents the proportional gain and T_i represents the integral time. For parameter tuning, this study uses the empirical Ziegler–Nichols (Z–N) method, which determines the PI parameters without complex mathematical calculations [26].

In this method, the integral value K_i is initially set to a very high value, and then K_p is gradually increased until the system reaches steady-state oscillation. This process is used to determine the ultimate gain K_u and the ultimate period P_u. The proportional gain of the PI controller based on the Ziegler–Nichols method is calculated using Equation (7).

$$K_p = 0.45 \times K_u \tag{7}$$

The ultimate period is obtained from the total oscillation time divided by the number of oscillations, as expressed in Equation (8).

$$P_u = \frac{T_{\text{total}}}{N} \tag{8}$$

After obtaining the ultimate period, the integral time constant is determined using Equation (9).

$$T_i = \frac{P_u}{1.2} \tag{9}$$

Finally, the integral gain is calculated from the proportional gain and integral time constant, as shown in Equation (10).

$$K_i = \frac{K_p}{T_i} \tag{10}$$

After the PI algorithm and tuning procedure have been described, the next subsection explains the simulation software used to model and evaluate the proposed system.

v. Power Simulator

Power Simulator (PSIM) is simulation software specifically designed for the analysis of power electronics systems, DC–DC converters, electric motor drives, power systems, and power control systems. PSIM provides fast and robust simulation algorithms [27]. Its main features include a schematic editor, a power component library consisting of MOSFETs, IGBTs, SCRs, diodes, inverters, and electric motors, a waveform viewer, an FFT analyzer for harmonic analysis, and current and voltage sensors for control systems. Compared to MATLAB/Simulink, PSIM offers significantly higher simulation speed for power electronics circuits [28].

After discussing the simulation platform, the next subsection describes the proposed CUK H-Bridge inverter topology modeled in PSIM.

vi. Design of a CUK H-Bridge Inverter

The proposed topology is divided into two sections. The first section is the H-Bridge inverter side with four active power switches, namely S_1–S_4, which convert DC voltage into AC voltage using a half-bridge rectification strategy. The second section is the AC CUK converter circuit, consisting of switches S_5–S_8, which regulates the voltage in buck-boost mode. Figure 4 shows the circuit diagram of the CUK H-Bridge inverter. The power switches used are IRFP460 MOSFETs, selected for their ability to operate at high voltage up to 500 V and maximum current of 20 A. The addition of an LC filter aims to reduce the THD value on the output current side [29].

The H-Bridge inverter is controlled by a zero-crossing Sinusoidal Pulse Width Modulation (SPWM)

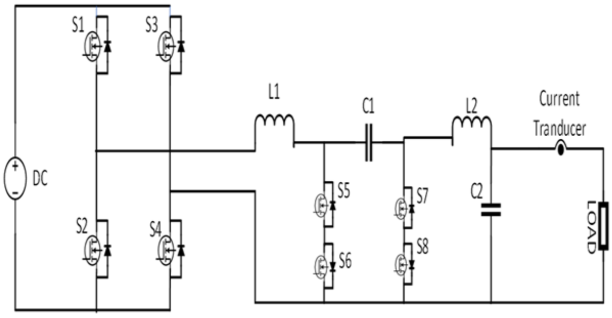

Figure 4: CUK H-Bridge inverter.

signal. To generate the SPWM waveform, a triangular carrier signal with a frequency of 10 kHz is required. This signal produces a 180° phase shift to form negative and positive cycles. Switches S_5–S_8 are controlled by a PWM signal to regulate the voltage in buck-boost mode. The PI controller is implemented using the TL084CN IC, which is a quad operational amplifier with 14 pins. The gain values are obtained using the Ziegler–Nichols method.

After the proposed topology has been defined, the next subsection presents the testing procedures and simulation parameters used to evaluate system performance.

vii. Testing Procedures

The tests were conducted through simulation using PSIM software. The first test was performed in open-loop mode to verify the input and output voltages under no-load conditions. Subsequently, a closed-loop test was conducted to control the current on the output side. The test parameters are presented in Table 2.

Table 2: Test parameters

Parameter	Value	Unit
V_{in}	50	VDC
Capacitor 1	4.7	μF
Capacitor 2	20	μF
Inductor 1	2	mH
Inductor 2	0.5	mH
Frequency	10	kHz
Load	10	Ω

A frequency of 10 kHz was selected as a compromise between power quality and switching losses. Higher frequencies can reduce the size of the LC filter, but they increase switching losses in the MOSFETs. In this study, the selected frequency of 10 kHz was able to achieve a THD of 3.6% in accordance with IEEE 519. Therefore, this frequency was considered sufficient to validate the performance of the proposed topology and control method.

Calibration of the PI parameters was performed using the Z–N method by gradually increasing K_p starting from 0.1, while observing the system response between the actual current I_{act} and the reference current I_{ref} at each step. After the ultimate gain was obtained, fine-tuning was performed using the trial-and-error method to improve system performance [30].

The passive component values were determined based on the analysis of the CUK converter operating modes under Continuous Conduction Mode (CCM) conditions. To determine the inductor value, the basic relationship between the inductor voltage and current variation is used, as expressed in Equation (11).

$$V_L = L\frac{di}{dt} \tag{11}$$

Equation (11) can be rearranged and integrated over the switching interval DT to obtain the inductor current ripple. The integration form is presented in Equation (12).

$$\Delta I_L = \int_0^{DT} \frac{V_L}{L}\,dt \tag{12}$$

Assuming that the inductor voltage remains constant during the switching interval, the inductor current ripple can be simplified as shown in Equation (13).

$$\Delta I_L = \frac{V_L DT}{L} \tag{13}$$

Since the switching period is defined as $T = 1/f_s$, the inductor current ripple can be rewritten in terms of switching frequency, as shown in Equation (14).

$$\Delta I_L = \frac{V_L D}{L f_s} \tag{14}$$

For the capacitor design, the relationship between capacitor current and voltage variation is used as the basis of the calculation. The basic capacitor current equation is expressed in Equation (15).

$$i_C = C\frac{dv}{dt} \tag{15}$$

Equation (15) can be rearranged and integrated over the switching interval DT to determine the capacitor voltage ripple. The integration form is shown in Equation (16).

$$\Delta V_C = \int_0^{DT} \frac{i_C}{C}\,dt \tag{16}$$

Assuming that the capacitor current is constant during the switching interval, the capacitor voltage ripple can be expressed as shown in Equation (17).

$$\Delta V_C = \frac{i_C DT}{C} \tag{17}$$

With the switching period defined as $T = 1/f_s$, the capacitor voltage ripple can be rewritten as a function of duty cycle and switching frequency, as expressed in Equation (18).

$$\Delta V_C = \frac{i_C D}{C f_s} \tag{18}$$

After obtaining the values of each passive component, the values were refined through trial-and-error simulations using PSIM to determine the optimal component values.

III. Results and Discussion

This section presents and discusses the simulation results of the proposed CUK H-Bridge current-controlled inverter. The evaluation includes open-loop switching verification, PI controller tuning, buck-boost operating mode analysis, power factor and output power assessment, and Total Harmonic Distortion (THD) analysis. Each result is analyzed to validate the performance of the proposed topology and the effectiveness of the PI-based current control strategy.

i. *Open-Loop Switching Verification*

In this study, preliminary testing was conducted using an open-loop simulation with Power Simulator (PSIM) software to verify that each circuit block, both on the power side and the control side, functioned normally prior to the integration of the closed-loop control system. This verification phase focused on observing the switching patterns and output waveforms at strategic measurement points defined in the model.

Based on observations on the H-Bridge inverter side, power switches S_1 and S_2 operate alternately and complement each other, while switches S_3 and S_4 function as zero-crossing switches, as shown in Figure 5. This switching pattern aligns with the Sinusoidal Pulse Width Modulation (SPWM) zero-crossing strategy, which utilizes a 10 kHz triangular carrier wave to produce a 180° phase shift, thereby precisely forming positive and negative cycles.

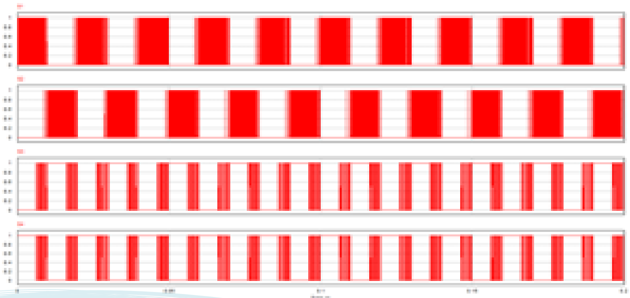

Figure 5: Switching pattern of the H-Bridge inverter.

In addition to verification on the switch side, measurements were taken at the inverter output voltage terminal V_o to ensure the integrity of the power system. The measurement results, as shown in Figure 6, indicate that although the output voltage is still in the form of a square wave, the waveform exhibits oscillatory characteristics that form a sinusoidal pattern. This technically indicates that the inverter side is functioning correctly.

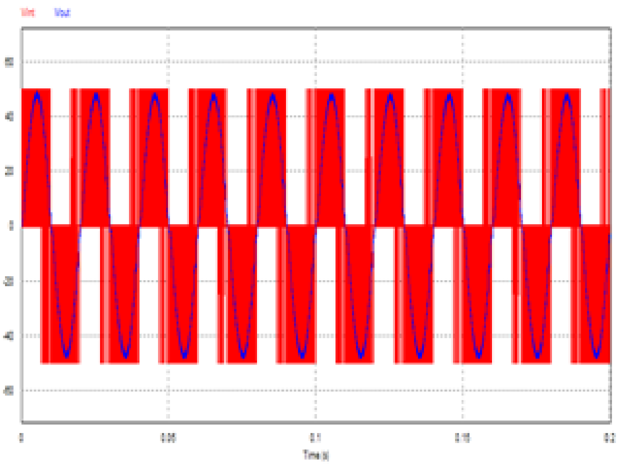

Figure 6: Output voltage of the H-Bridge inverter.

Verification then continued on the boost converter section by placing probes on switches Q_1 through Q_4, as shown in Figure 7. The simulation results confirm that each switch on the converter side turns on alternately in accordance with the given PWM signal, proving that the entire power circuit is ready to operate in current control mode based on the Proportional-Integral (PI) algorithm.

The output of the PI controller is a control signal representing the current error between I_{ref} and I_{act}. This signal is compared with a 10 kHz triangular carrier wave to generate PWM. The resulting PWM duty cycle is then used to control switches S_5–S_8 in the CUK section of the AC–AC converter.

Thus, changes in the current error directly affect the duty cycle of switches S_5–S_8, so that the output voltage can be regulated in both buck and boost modes. No dead-time has been explicitly implemented in the simulation model. The simulation uses ideal complementary PWM signals so that there is no overlap between pairs of switches operating in opposite directions. Therefore, shoot-through conditions do not occur in the simulation environment. However, in real hardware implementations, dead-time must be added to the gate signals to account for the turn-on and turn-off delays of the MOSFETs, which can cause shoot-through.

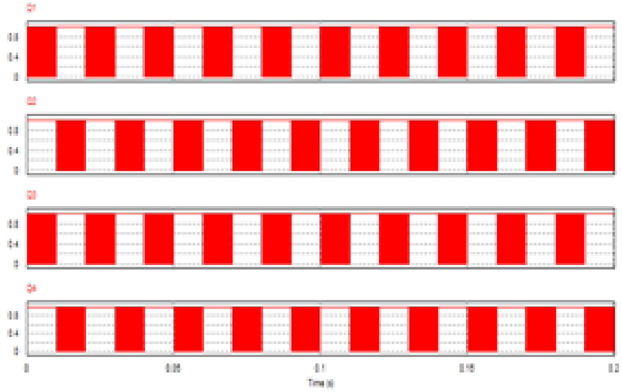

Figure 7: Switching pattern of Q_1–Q_4.

ii. PI Controller Tuning

In the next stage of this study, the Proportional-Integral (PI) controller was tuned to ensure system stability in controlling the output current. This tuning process uses the empirical Ziegler–Nichols (Z–N) method, in which the proportional gain K_p is gradually increased while the integral parameter T_i is set to a high value of $T_i = 1000$. This condition is used to focus the observation solely on the effect of the proportional parameter.

In the initial experiment with $K_p = 0.1$, the system demonstrated the ability to track the reference current I_{ref}, but with a very slow response characterized by a large amplitude difference between the actual current I_{act} and the reference current. The comparison between I_{ref} and I_{act} during PI tuning is shown in Figure 8.

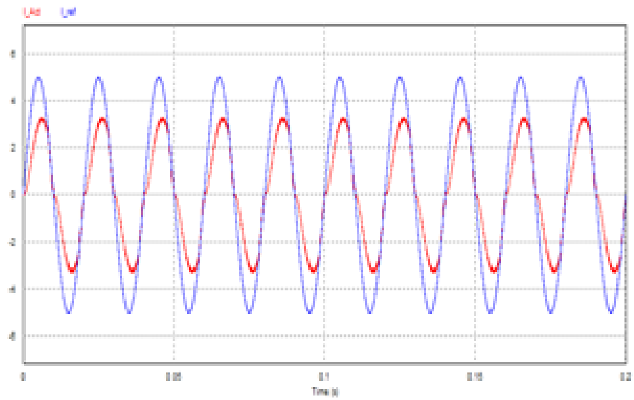

Figure 8: Comparison between I_{ref} and I_{act} during PI tuning.

Gradually increasing the K_p value to 0.3 and 0.5 improves tracking performance and speeds up the system response, although the amplitude error has not yet been completely eliminated. Figure 9 shows the condition when K_p reaches 0.8. Under this condition, the system exhibits increasingly stable behavior with reduced error, eventually reaching the final gain K_u at $K_p = 1$. At this point, the system achieves steady-state stability with no error and a final period P_u of 0.02 s.

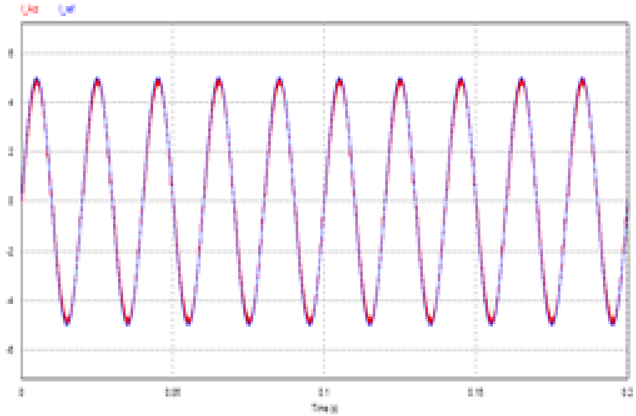

Figure 9: Comparison between I_{ref} and I_{act} under K_u condition.

Based on the obtained K_u and P_u values, calculations using the standard Ziegler–Nichols equation yielded initial parameters of $K_p = 0.45$, $K_i = 27$, and $T_i = 0.0167$. Although these parameters provided a good control foundation, this study proceeded to a refinement stage through a trial-and-error adjustment process to achieve more accurate performance. As shown in Figure 10, the final results of this adjustment established optimal values of $K_p = 0.6$, $T_i = 0.0167$, and $K_i = 35$.

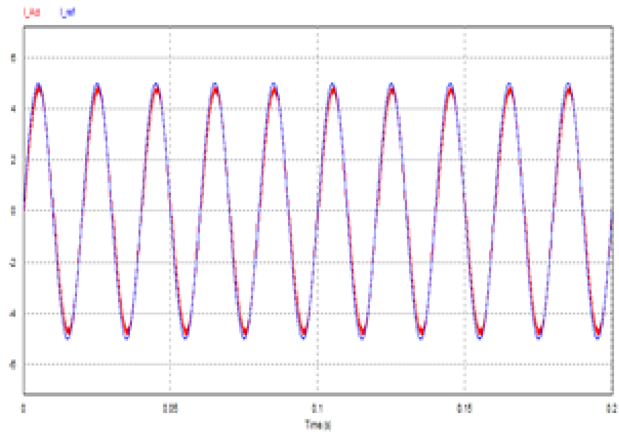

Figure 10: Condition of I_{ref} and I_{act} after fine-tuning.

The results in Figure 10 confirm that although the Ziegler–Nichols method is highly effective as a practical initial approach, further adjustments are still necessary to achieve the most optimal and accurate operating point for the system in this CUK H-Bridge Inverter simulation.

iii. Tests for Buck-Boost Mode

Another stage of testing focused on evaluating the output voltage V_o performance in response to variations in the reference current I_{ref} to validate the operational flexibility of the CUK H-Bridge Inverter topology. The testing was conducted by maintaining a constant input voltage V_{in} of 50 VDC, which serves as a reference for determining the system operating mode. Mode determination is based on a comparison between V_o and V_{in}, where the system operates in buck mode if $V_o < V_{in}$ and in boost mode if $V_o > V_{in}$. The test parameters using the reference current are summarized in Table 3.

Table 3: Buck-boost mode test parameters

I_{ref} **(A)**	V_o **(V)**	**Mode**
3	30	Buck
5	50	Steady state
10	100	Boost

Based on the simulation results presented in Table 3, when the reference current is set to 3 A, this topology operates in buck mode with an output voltage of 30 V. When the current is increased to 5 A, the system reaches a steady-state condition where V_o oscillates around 50 V, equivalent to the input voltage. A significant change occurs when the reference current is further increased; at 10 A, the topology switches to boost mode with V_o reaching 100 V, or twice the value of V_{in}. Figure 11 shows the results of the buck-boost mode test.

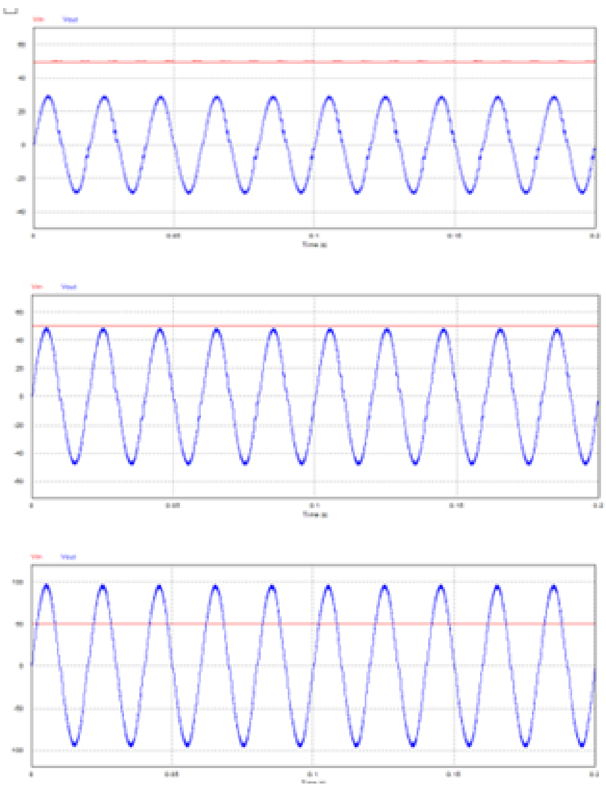

Figure 11: Output voltage during buck-boost mode testing.

The results in Figure 11 empirically confirm that the output current is directly proportional to the output voltage, such that an increase in the reference current proportionally increases the voltage level at the load terminals. The success of the transition between these modes is heavily influenced by the role of the passive components used in the design. Coupling capacitor C_1 plays a crucial role in transferring energy to the output side, while capacitor C_2 and inductor L_2 act as filters to reduce ripple and maintain output stability in each mode.

Additionally, inductor L_1 on the input side ensures continuous voltage by storing energy from the source. The system ability to accurately track the actual current at various operating points demonstrates that the combination of the CUK H-Bridge topology and the applied control algorithm is effective for applications requiring flexible voltage regulation.

iv. Power Factor and Output Power

This test focuses on analyzing the correlation between the phase of the output voltage V_o and the actual current I_{act} to determine the system power transfer efficiency. Measurement results from the same channel on the waveform display show that the V_o and I_{act} waveforms are in phase, with the peaks and troughs of both waveforms occurring simultaneously. This phase alignment is due to the use of a resistive load in the simulation test parameters.

Due to the absence of phase shift between voltage and current, the system successfully achieves a highly optimal power factor, represented by $\cos\phi$, approaching unity. The power factor result of the proposed topology is shown in Figure 12.

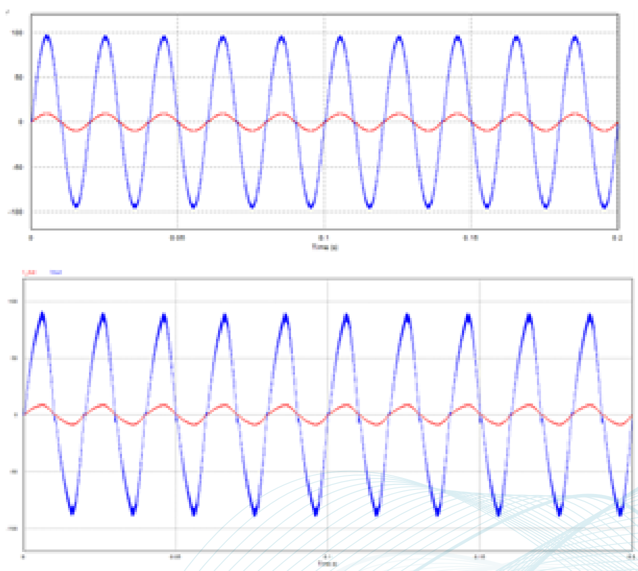

Figure 12: Power factor value of the proposed topology.

Meanwhile, the topology was also subjected to an inductive load in the form of a transformer. This resulted in a reduction in the output voltage amplitude as well as a current lag relative to the voltage. Although the waveform remains sinusoidal, the energy stored in the magnetic field results in a lower power factor compared to a resistive load. A comparison of the resistive and inductive load tests is presented in Table 4.

Table 4: Load comparison

Parameter	Resistive Load	Inductive Load (Transformer)
Phase shifting	0°	Lagging
Power factor	≈ 1	< 1
Voltage amplitude	± 95 V	± 90 V
Waveform	Stable sinusoidal	Sinusoidal with slight amplitude reduction

As shown in Table 4, the resistive load produces no phase shift between voltage and current, resulting in a power factor close to unity. In contrast, the inductive load produces a lagging current response and a lower power factor.

In terms of power capacity performance, the designed CUK H-Bridge Inverter topology demonstrates the ability to handle high-power loads. Based on the test data, the maximum output power that the system can generate is 2250 W or 2.25 kW. This peak power is achieved at a maximum reference current of 15 A with an output voltage of 150 V in boost mode.

Technically, the magnitude of this output power is highly dependent on the selection of passive component values used in the modeling, particularly the characteristics of the load resistor as well as the capacitance of the filter capacitor and coupling capacitors C_1 and C_2. The success in achieving 2.25 kW of power with an ideal power factor demonstrates that the integration of the CUK topology and the H-Bridge inverter offers advantages in stability and power capacity compared to other conventional topologies.

v. THD Analysis

In the final stage of system performance evaluation, power quality was assessed by measuring the Total Harmonic Distortion (THD) value of the output current. This parameter is crucial because the power quality of a converter significantly affects the performance and service life of components in the entire electrical system. In power electronics industry standards, IEEE 519 specifies that the maximum allowable THD value for connected systems is 5%.

Before conducting the harmonic analysis, the output current waveform of the proposed topology was first observed to evaluate the sinusoidal characteristics of the current signal, as shown in Figure 13. The waveform indicates that the PI-controlled CUK H-Bridge inverter is able to produce a stable output current with a shape approaching a sinusoidal waveform.

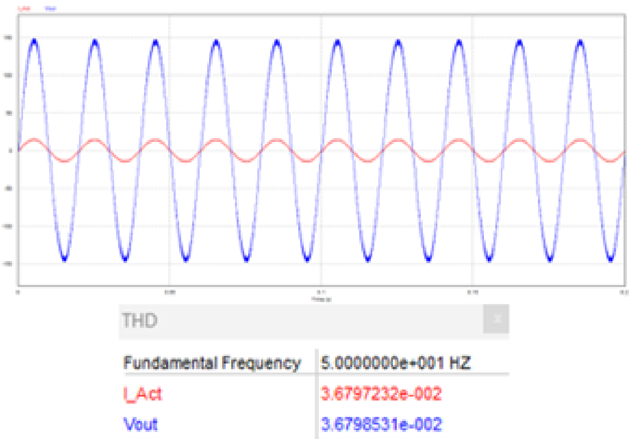

Figure 13: Output current waveform of the proposed topology.

Based on the harmonic analysis shown in Figure 14, the proposed CUK H-Bridge Inverter topology successfully achieved an output current THD value of 3.6%. This value is below the IEEE 519 standard threshold, indicating that the output current has excellent quality and a low distortion level.

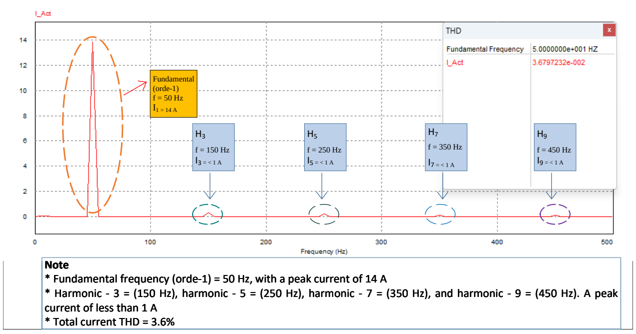

Figure 14: THD value of the proposed topology.

The result in Figure 14 demonstrates the effectiveness of the integration between the passive components and the implemented control algorithm in reducing harmonic distortion. Technically, the use of an LC filter consisting of inductor L_2 and capacitor C_2 plays a vital role in filtering current and voltage ripple, resulting in a smoother waveform that approaches a pure sine wave. Additionally, the use of a Proportional-Integral (PI) control algorithm that has undergone fine-tuning effectively minimizes tracking error in the output current, which directly contributes to the reduction of system harmonics.

Thus, the combination of the PI-controlled CUK H-Bridge Inverter topology has proven capable of producing reliable power conversion and meeting international power quality regulations for renewable energy applications.

IV. Conclusion

The topology design of the CUK H-Bridge Inverter has been successfully carried out by combining an H-Bridge inverter and a CUK converter, equipped with an LC filter and a closed-loop PI control system, which was simulated using PSIM software. This topology converts DC voltage into AC voltage through the inverter, then regulates the voltage and current levels using the CUK converter in buck and boost modes. The system is controlled by the PI controller to produce stable voltage and high-quality current.

The Proportional-Integral (PI) control algorithm, tuned using the Ziegler–Nichols method and further refined through fine-tuning to obtain $K_p = 0.6$ and $K_i = 35$, is capable of minimizing the error between the reference current and the actual current. The controller produces a fast system response and eliminates steady-state error. The output current accurately tracks the reference across the entire operating range, with a THD of 3.6% that meets the IEEE 519 standard, and a maximum output power of 2.25 kW at 150 V.

Further research is recommended for several aspects: implementing a hardware prototype to validate the simulation results; adding a harmonic filter on the output side to further reduce THD; investigating more advanced control algorithms such as Fuzzy Logic, Model Predictive Control (MPC), or Sliding Mode Control; and integrating the topology with renewable energy sources, such as solar panels, for grid-connected or off-grid applications.

Acknowledgment

The author would like to express gratitude to Sultan Agung Islamic University (UNISSULA) in Semarang for the facilities and support provided throughout this research.

References

[1] A. N. Sonjaya, D. Marpaung, S. W. Lestari, N. W. Yanto, and Y. Widyawati, "Potensi energi terbarukan di sumatra tahun 2020–2050 menggunakan long-range energy alternatives planning system (leap)," *Jurnal Teknologi*, vol. 11, no. 1, pp. 36–57, 2023. https://doi.org/10.31479/jtek.v11i1.277

[2] J. L. Holechek, H. M. E. Geli, M. N. Sawalhah, and R. Valdez, "A global assessment: Can renewable energy replace fossil fuels by 2050?" *Sustainability*, vol. 14, no. 8, pp. 1–22, 2022. https://doi.org/10.3390/su14084792

[3] N. K. A. Kalair, N. Abas, M. S. Saleem, and A. R. Kalair, "Role of energy storage systems in energy transition from fossil fuels to renewables," *Energy Storage*, vol. 3, no. 1, pp. 1–27, 2021. https://doi.org/10.1002/est2.135

[4] Neha and J. Rambeer, "Renewable energy sources: A review," *Journal of Physics: Conference Series*, vol. 1979, no. 1, 2021. https://doi.org/10.1088/1742-6596/1979/1/012023

[5] R. Aravind, B. Chokkalingam, R. Verma, S. Aruchamy, and L. Mihet-Popa, "Multi-port non-isolated dc-dc converters and their control techniques for the applications of renewable energy," *IEEE Access*, vol. 12, pp. 88 458–88 491, 2024. https://doi.org/10.1109/ACCESS.2024.3413354

[6] Ardiansa and A. A. Akbar, "Perancangan alat pengubah arus dc ke ac berbasis mikrokontroler sebagai pengganti pagar kebun," *Antivirus: Jurnal Ilmiah Teknik Informatika*, vol. 15, no. 2, pp. 199–208, 2021. https://doi.org/10.35457/antivirus.v15i2.1721

[7] D. B. R. et al., "Grid forming inverter modeling, control, and applications," *IEEE Access*, vol. 9, pp. 114 781–114 807, 2021. https://doi.org/10.1109/ACCESS.2021.3104617

[8] F., S. S., and K. T. H. Babu, "A single-phase coupled inductor-based buck-boost inverter," in *Proceedings of the 1st International Conference on Innovation in Information and Communication Technology*, 2019.

[9] K. Kim, H. Cha, and H. G. Kim, "A new single-phase switched-coupled-inductor dc-ac inverter for photovoltaic systems," *IEEE Transactions on Power Electronics*, vol. 32, no. 7, pp. 5016–5022, 2017. https://doi.org/10.1109/TPEL.2016.2606489

[10] H. N. Hermala, S. Riyadi, L. H. Pratomo, F. B. Setiawan, and A. Wibisono, "Design and implementation of digital hysteresis control in a sepic buck-boost converter topology," *Riset dan Teknologi Terapan*, pp. 1–10, 2021. https://journal.unpar.ac.id/index.php/ritektra/article/view/4929

[11] M. P. et al., "An alternative level enhanced switching angle modulation schemes for cascaded h bridge multilevel inverters," *IEEE Access*, vol. 11, pp. 57 365–57 382, 2023. https://doi.org/10.1109/ACCESS.2023.3283253

[12] S. S. B. and S. Behera, "An optimize configuration of h-bridge multivel inverter," in *Proceedings of the 2021 1st International Conference on Power Electronics and Energy*, 2021, pp. 1–4. https://doi.org/10.1109/ICPEE50452.2021.9358533

[13] M. Meraj, S. Rahman, A. Iqbal, and L. Ben-Brahim, "Common mode voltage reduction in a single-phase quasi z-source inverter for transformerless grid-connected solar pv applications," *IEEE Journal of Emerging and Selected Topics in Power Electronics*, vol. 7, no. 2, pp. 1352–1363, 2019. https://doi.org/10.1109/JESTPE.2018.2867521

[14] G. C. Anggoro and L. H. Pratomo, "Design and implementation of cuk h-bridge inverter voltage control using stm32f407vet6," *ELKOMIKA: Jurnal Teknik Energi Elektrik, Teknik Telekomunikasi, dan Teknik Elektronika*, vol. 13, no. 3, p. 286, 2025. https://doi.org/10.26760/elkomika.v13i3.286

[15] M. Munir, "Analisis inverter dengan konverter cuk yang dimodifikasi sebagai sel dasar," Master's thesis, Institut Teknologi Bandung, 2023.

[16] A. Wibisono, S. Riyadi, and A. Martanio, "Desain dan implementasi kendali digital proportional-integral pada cuk converter," *Majalah Ilmiah Teknologi Elektro*, vol. 21, no. 1, p. 149, 2022. https://doi.org/10.24843/mite.2022.v21i01.p20

[17] S. K. Peddapelli, *Pulse Width Modulation: Analysis and Performance in Multi-Level Inverters*. Boston: De Gruyter Oldenbourg, 2007.

[18] R. A. Igam, A. Lomi, and A. U. Krismanto, "Rancang bangun dc/dc cuk converter berbasis fuzzy logic control untuk kendali baterai pada plts skala kecil," *Jurnal Magnetika*, vol. 2, no. 2, pp. 1–12, 2024. https://garuda.kemdiktisaintek.go.id/journal/view/36725?page=9

[19] I. Ferdiansyah, I. Sudiharto, and E. Sunarno, "Desain spwm single phase full bridge inverter pada sistem uninterruptible power supply 500w," *Jurnal Arus Elektro Indonesia*, vol. 7, no. 1, 2021. https://doi.org/10.19184/jaei.v7i1.23438

[20] T. B. G. Azmi, A. P. Susanto, A. N. Zakariya, and D. O. Radianto, "Analisis perbandingan efisiensi buck-boost converter dengan cuk converter pada panel surya," *Koloni*, vol. 3, no. 2, pp. 82–87, 2024. https://doi.org/10.31004/koloni.v3i2.622

[21] B. K. Kushwaha and A. Narain, "Controller design for cuk converter using model order reduction," in *Proceedings of the 2012 2nd International Conference on Power, Control and Embedded Systems*, 2012, pp. 1–5. https://doi.org/10.1109/ICPCES.2012.6508134

[22] A. Anand and B. Singh, "Modified dual output cuk converter-fed switched reluctance motor drive with power factor correction," *IEEE Transactions on Power Electronics*, vol. 34, no. 1, pp. 624–635, 2019. https://doi.org/10.1109/TPEL.2018.2827048

[23] K. A. Mahafzah, A. Q. Al-Shetwi, M. A. Hannan, T. S. Babu, and N. Nwulu, "A new cuk-based dc-dc converter with improved efficiency and lower rated voltage of coupling capacitor," *Sustainability*, vol. 15, no. 11, 2023. https://doi.org/10.3390/su15118515

[24] A. Elnady, A. A. A. Ismail, M. Alshabi, and A. Noureldin, "A comprehensive review of centralized current/power control schemes for parallel inverters and ac microgrids," *IEEE Access*, vol. 10, pp. 125 061–125 085, 2022. https://doi.org/10.1109/ACCESS.2022.3222315

[25] L. H. Pratomo and H. D. E. Christiawan, "Pengendalian arus pada inverter lima tingkat penaik dan penurun tegangan," *ELKOMIKA*, vol. 11, no. 3, p. 783, 2023. https://doi.org/10.26760/elkomika.v11i3.783

[26] Y. Gao and W. Zhu, "A segmented adaptive pid temperature control method suitable for industrial dispensing system," *Electronics*, vol. 14, no. 11, p. 2306, 2025. https://doi.org/10.3390/electronics14112306

[27] M. Y. Hammoudi, O. Kraa, R. Saadi, M. Y. Ayad, S. Bacha, and A. Boukhlouf, "Non linear control of a fuel cell interleaved boost converter using weighted mixed sensitivity h-infinity," in *Proceedings of the 2018 3rd International Conference on Electrical Sciences and Technologies in Maghreb*, 2018, pp. 1–5. https://doi.org/10.1109/CISTEM.2018.8613563

[28] G. Sun, J. Sun, J. Zhang, and S. Li, "Based on psim software energy feedback-based power electronic load model," in *Proceedings of the 2011 International Conference on Electrical and Control Engineering*, 2011, pp. 3852–3855. https://doi.org/10.1109/ICECENG.2011.6057927

[29] C. Bai, B. Han, and M. Kim, "Current-fed dual-half-bridge converter directly connected with half-bridge inverter for residential photovoltaic system," *Solar Energy*, vol. 174, pp. 108–120, 2018. https://doi.org/10.1016/j.solener.2018.08.039

[30] S. Surya and V. Patil, "Cuk converter as an efficient driver for led," in *Proceedings of the 4th International Conference on Electrical, Electronics, Communication, Computer Technologies and Optimization Techniques*, 2019, pp. 49–52. https://doi.org/10.1109/ICEECCOT46775.2019.9114648